JACC Vol. 7, No. 2
February 1986:317–26

Quantitative Assessment of Regional Left Ventricular Motion Using Endocardial Landmarks

CORNELIS J. SLAGER, MSc, TON E. H. HOOGHOUDT, MD,* PATRICK W. SERRUYS, MD, JOHAN C. H. SCHUURBIERS, BSc, JOHAN H. C. REIBER, PhD, GEERT T. MEESTER, MD, FACC, PIETER D. VERDOUW, PhD, PAUL G. HUGENHOLTZ, MD, FACC

Rotterdam, The Netherlands

In this study the hypothesis is tested that the motion pattern of small anatomic landmarks, recognizable at the left ventricular endocardial border in the contrast angiocardiogram, reflects the motion of the endocardial wall. To verify this, minute metal markers were inserted in the endocardium of eight pigs with a novel retrograde transvascular approach. Marker motion was subsequently recorded with roentgen cinematography and compared with the motion of the landmarks on the endocardial contours detected from the contrast ventriculogram with an automated contour detection system. Linear regression analysis of the directions of the systolic metal marker and endocardial landmark pathways yielded a correlation coefficient of 0.86 and a standard error of the estimate of 10.3°.

Landmark pathways were also measured in 23 normal human left ventriculograms. Normal left ventricular endocardial wall motion during systole, as observed in the 30° right anterior oblique view, is characterized by a dominant inward transverse motion of the opposite anterior and inferoposterior walls and a descent of the base toward the apex. The apex itself is almost stationary. On the basis of these observations, a widely applicable model for the assessment of left ventricular wall motion is described in mathematical terms.

(J Am Coll Cardiol 1986;7:317–26)

The very existence of several methods (1–6) to analyze left ventricular wall motion from contrast angiograms indicates that no exact, generally accepted procedure is available to track fixed points along the endocardial wall. In animals, specific sites of the endocardium can easily be followed with endocardially implanted metal clips (7–9) and roentgen cinematography. For obvious reasons, endocardial markers have not been inserted in humans, although midwall motion (10) and epicardial wall motion (11–13) have been studied in human hearts with surgically implanted metal markers. However, major differences exist in extent and direction among the movements of neighboring endocardial, midwall and epicardial sites as the wall thickens (7,14). Therefore, none of these methods can provide an accurate description of endocardial wall motion.

In this study a method is described and evaluated to assess left ventricular endocardial wall motion in humans from the pathways of anatomic landmarks recognizable on the endocardial border. For delineation of the endocardial border in the contrast angiogram, an automated high resolution outlining system (15) was employed. In the detected left ventricular contour, small landmarks are available that can be followed throughout the cardiac cycle by analysis of consecutive frames of the cineangiogram. The hypothesis that these landmarks represent specific anatomic sites has been validated by placing minute "harpoons" in the endocardium of piglets. By comparing the mean systolic pathways of these artificial landmarks with those naturally occurring, their usefulness could be substantiated.

Subsequently, the naturally occurring landmarks in normal human individuals were determined from left ventricular cineangiograms, and a widely applicable model for the assessment of human left ventricular wall motion was derived. The applicability of this model is illustrated with use of the results of wall motion analysis of a left ventricle filmed during a coronary balloon dilation procedure.

Methods

Animal study. The first study group consisted of eight anesthetized pigs with a mean weight of 24 kg. Left ven-

From the Thoraxcenter, Erasmus University and University Hospital Dijkzigt, Rotterdam, The Netherlands.

Manuscript received July 3, 1984; revised manuscript received August 20, 1985, accepted September 3, 1985.

*Present address: Canisius Hospital, Nijmegen, The Netherlands.

Address for reprints: Cornelis J. Slager, MSc, Thoraxcenter, Ee 2322, Erasmus University Rotterdam, PO Box 1738, 3000 DR Rotterdam, The Netherlands.

0735-1097/86/$3.50

JACC Vol. 7, No. 2
February 1986:317–26

tricular pressure was obtained from a micromanometer-tipped catheter. A pacing catheter was introduced into the coronary sinus. A fixed heart rate 10 beats/min above heart rate at rest was chosen and maintained during the study. A left ventriculogram was made during injection of 0.75 ml/kg meglumine diatrizoate (Urografin 76) through an 8F angiocatheter at a rate of 12 ml/s. The opacified ventricle was filmed in the left lateral projection at a rate of 50 frames/s. During angiography, artificial respiration was stopped to exclude extracardiac motion. After the acquisition of a technically satisfactory cineangiogram, specific sites of the endocardial wall were marked with small metal darts or "miniharpoons." For this purpose a spring-loaded insertion device (Fig. 1) attached to the tip of a flexible catheter with tip-steering capability (Muller Guide System and Variflex 7F catheter, USCI) was used. The combination of the sharp barbed hook and a blunt body guarantees excellent fixation of the marker with minimal damage to the myocardium and accurate delineation of the endocardium. In each pig five markers were inserted along the anterior and inferoposterior walls of the left ventricle in a pattern outlining the ventricular cavity, as seen in the left lateral projection (Fig. 2). To detect possible myocardial injury due to the insertion procedure, the electrocardiogram and left ventricular pressure were monitored continuously. Once the markers were inserted, a second left ventricular angiogram was taken with identical X-ray configuration and with the respirator turned off. A centimeter grid was filmed for calibration purposes and an interval of at least 30 minutes was observed between the consecutive angiograms.

Patient group: ventriculography. The second study group consisted of 23 patients who underwent diagnostic heart catheterization because of suspected heart disease and who appeared to have no hemodynamic or angiocardiographic abnormality. Patients were studied after an overnight fast without premedication; all drugs that might influence left ventricular contractile function were discontinued at least 24 hours before the study. Left ventricular cine-

Figure 1. Schematic drawing and photograph of spring-loaded metal marker insertion device attached to the tip of a 7F catheter. The inner tube, including spring B, metal marker C and trigger lever D, is advanced by manual injection of saline solution into catheter A until D snaps back into hole E of the outer tube. Then B shoots off C.

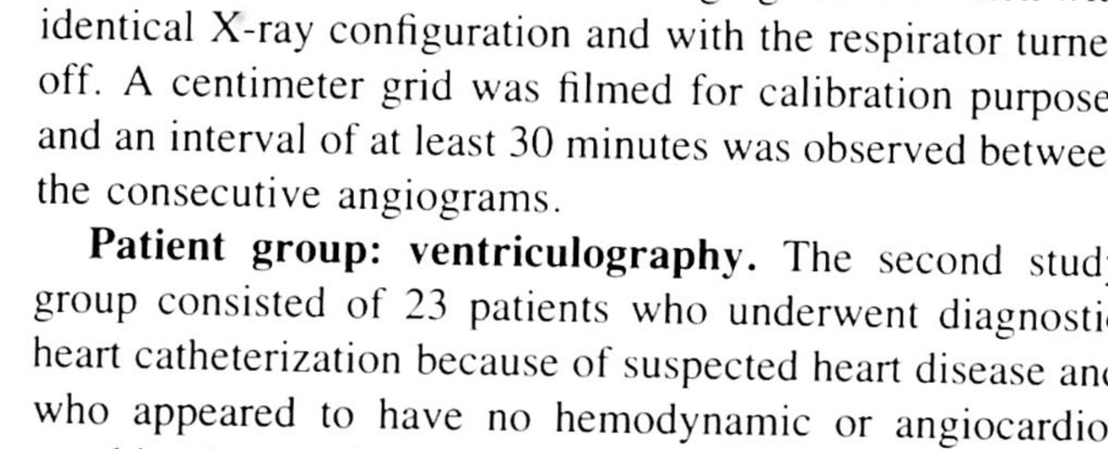

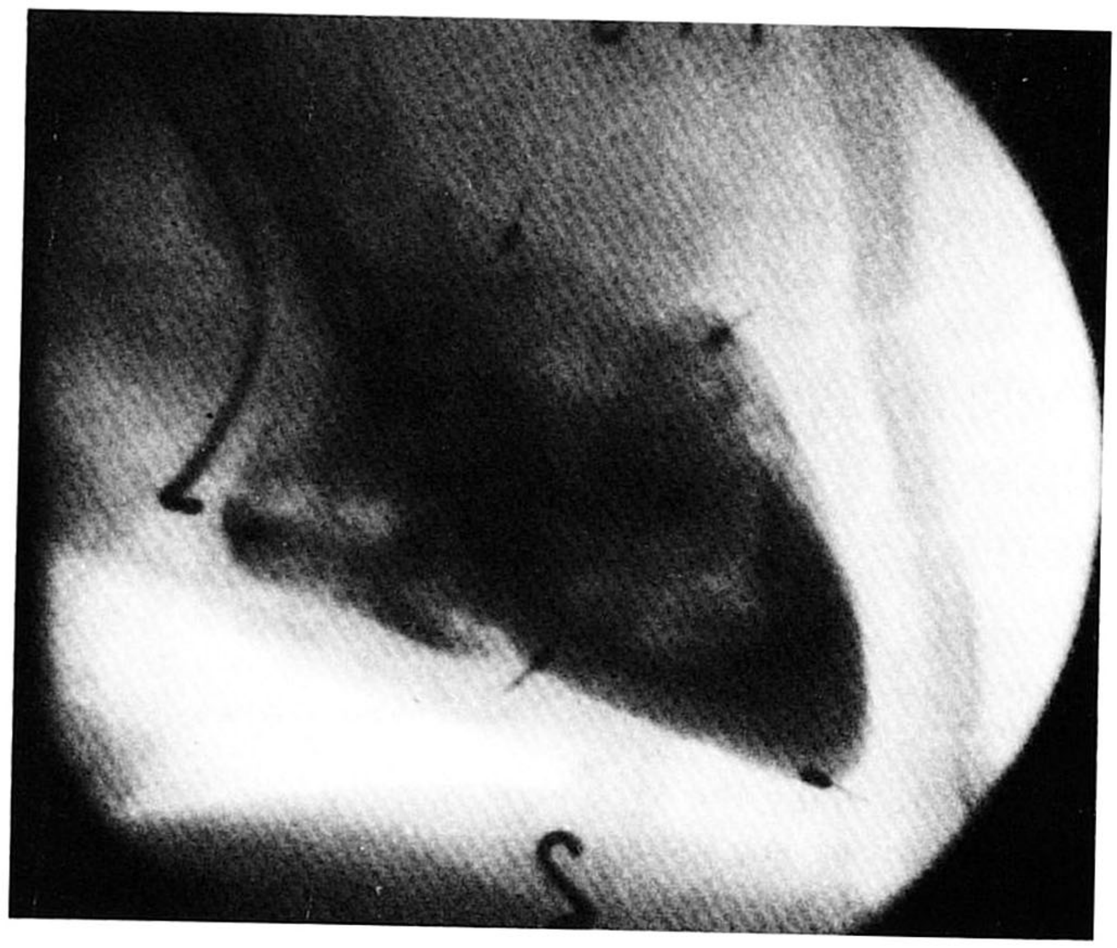

Figure 2. End-diastolic frame from a left ventricular angiogram in a pig; metal markers outline the left ventricular cavity as seen in the left lateral projection.

angiography was performed at heart rate at rest, during injection of 0.75 mg/kg Urografin 76 at a rate of 16 to 18 ml/s. The 30° right anterior oblique projection of the opacified ventricle was filmed at a rate of 50 frames/s. During angiography, care was taken that the patient maintained a steady position with regard to the X-ray equipment and suspended respiration to prevent respiratory motion. For calibration purposes a centimeter grid was filmed at mid-thoracic level.

Analysis of ventriculograms. The endocardial outlines of both the human and pig contrast angiograms were determined on a frame by frame basis with the Contouromat, an automated contour detection system (15). In each frame left ventricular volume was determined according to Simpson's rule (16). End-diastole and end-systole were defined as the moments of maximal and minimal left ventricular volume, respectively. The detected contours of all systolic frames were displayed on a video monitor and collectively recorded on a single 8.3 × 10.8 cm Polaroid photograph. The contours were displayed as detected from the cine-frames; that is, a fixed external reference system (5) was employed and no translational or rotational "correction" procedures were applied. On this contour graph the pathways of small landmarks at various sites along the left ventricular contrast border can be recognized through substantial parts of the systolic period; however, the information may be partially obscured by the overlap of successive contours. To eliminate such superimposition, a "shift" procedure (17) was applied to the detected contours (Fig. 3A). After photographic enlargement of the shifted contours, the local directions of the recognizable landmark pathways were indicated manually (Fig. 3B). Subsequent interpolation be-

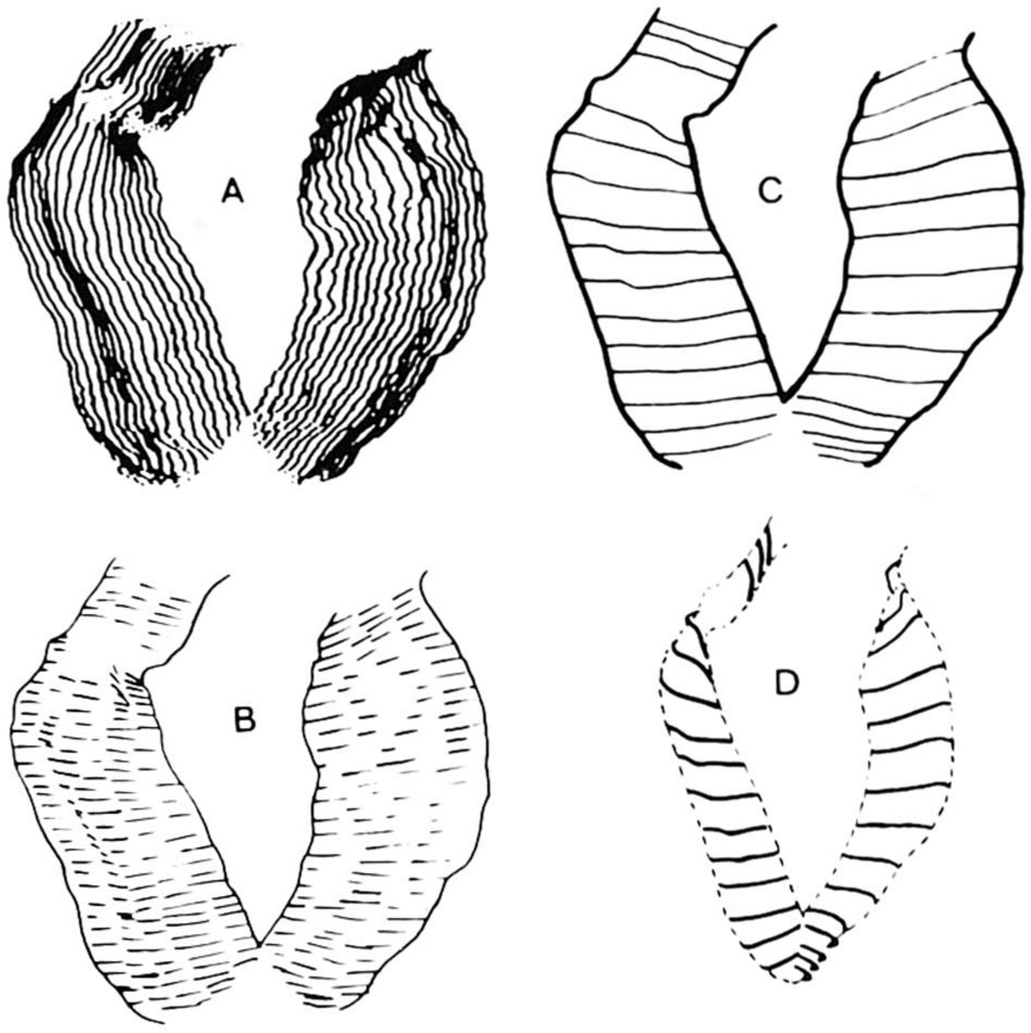

Figure 3. A, Automated frame by frame analysis of the shifted endocardial contours in the systolic period from a left ventricular cineangiocardiogram. **B,** Pathways of small anatomic landmarks at the left ventricular contrast border are indicated, which results in a pattern of trajectories. **C,** Interpolation between neighboring pathways allows definition of a set of trajectories covering the whole systolic period. **D,** Correction for the previously added shift yields the actual endocardial landmark motion with respect to the original frame of reference.

tween the indicated neighboring pathway directions allowed one to track the systolic pathway of the endocardium at an arbitrarily chosen number of sites (Fig. 3C). Finally, correction for the previously added shift yielded a set of actual systolic trajectories projected onto the original frame of reference (Fig. 3D).

The pig contrast angiocardiograms obtained after implantation of the metal markers were projected on paper. The end-diastolic and end-systolic contours were drawn manually and the positions of the markers were indicated. In subsequent calculations the curved systolic landmark and marker trajectories were represented by straight vectors connecting the end-diastolic with the end-systolic positions, respectively.

Coordinate system. For subsequent quantitative analysis a nonindexed rectangular coordinate system was defined on the basis of the end-diastolic contour. The origin coincides with the end-diastolic apex, the point at maximal distance from the superior aspect of the aortic valve (18). A basal transverse axis, extending from the mitral valve fornix to a point on the opposite anterior wall, was constructed, creating an isosceles triangle with its vertex at the ventricular apex (Fig. 4). The ventricular long axis was defined as the median of this triangle through the vertex; the y axis of the coordinate system coincides with this line.

Normalization. A normalization procedure was carried out to compare the pathways at various endocardial sites of ventricles with different shapes and sizes. First, 10 equidistant points were defined along the long axis. Lines drawn through these points in a direction perpendicular to the long axis defined a total of 20 intersecting points with the end-diastolic contour (Fig. 4). These 20 points were considered to be the initial end-diastolic endocardial sites to be used in assessing the interpolated pathways of the previously mentioned landmarks. For both the human and pig ventricles, left ventricular dimensions were normalized so that for each study group the end-diastolic long-axis lengths became equal to the mean value. As a result of this procedure, corresponding sites had equal y coordinates but still unequal x coordinates. Finally, the normalized systolic trajectories at corresponding sites were shifted parallel to the x axis so that they coincided with the mean value of the individual x coordinates (Fig. 5).

With respect to the coordinate system, the individual pathways were decomposed into their x and y components, expressed as Δx and Δy. The direction of each pathway was defined as the acute angle (α) between the pathway and the x axis: $\alpha = \text{arc tan} \frac{|\Delta x|}{y}$, where arc tan = arc tangent

Figure 4. The median of an isosceles triangle, with its vertex at the ventricular apex and its base extending from the mitral valve fornix, defines the y axis of a rectangular coordinate system. Left ventricular long-axis (LA) length is defined as the distance from base to apex. From base to apex at equidistant y levels, 20 end-diastolic starting points are defined for the assessment of pathways of the endocardial landmarks. α = the acute angle; x = x coordinate.

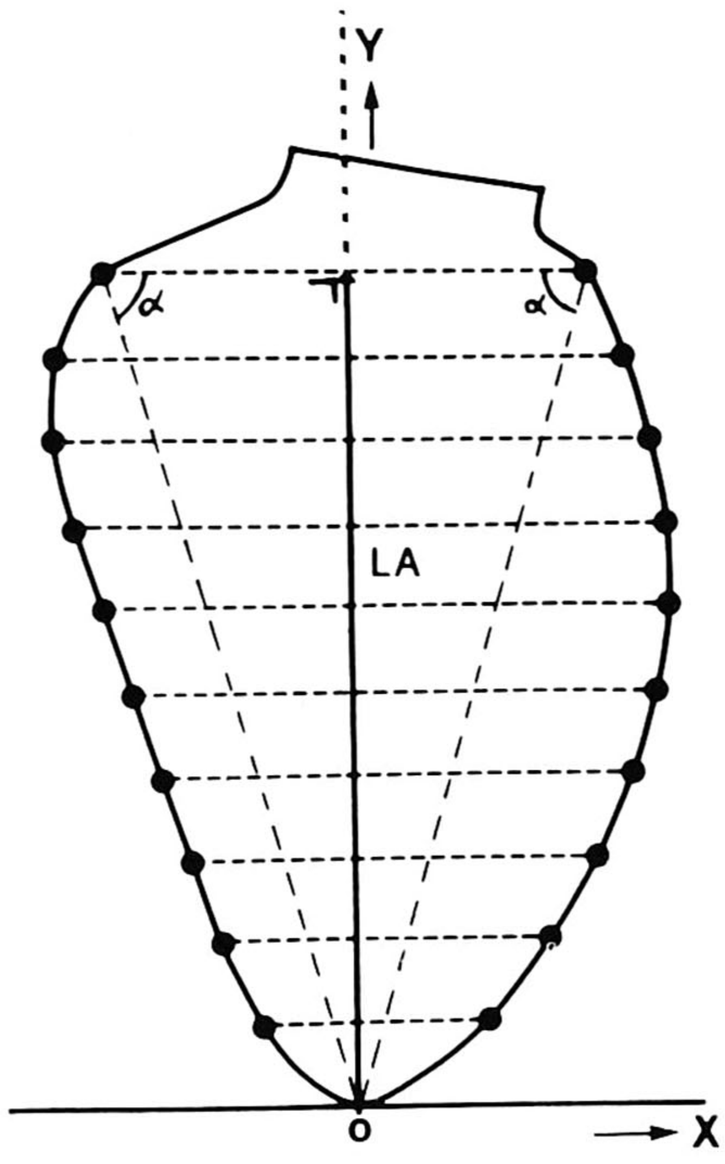

JACC Vol. 7, No. 2
February 1986:317–26

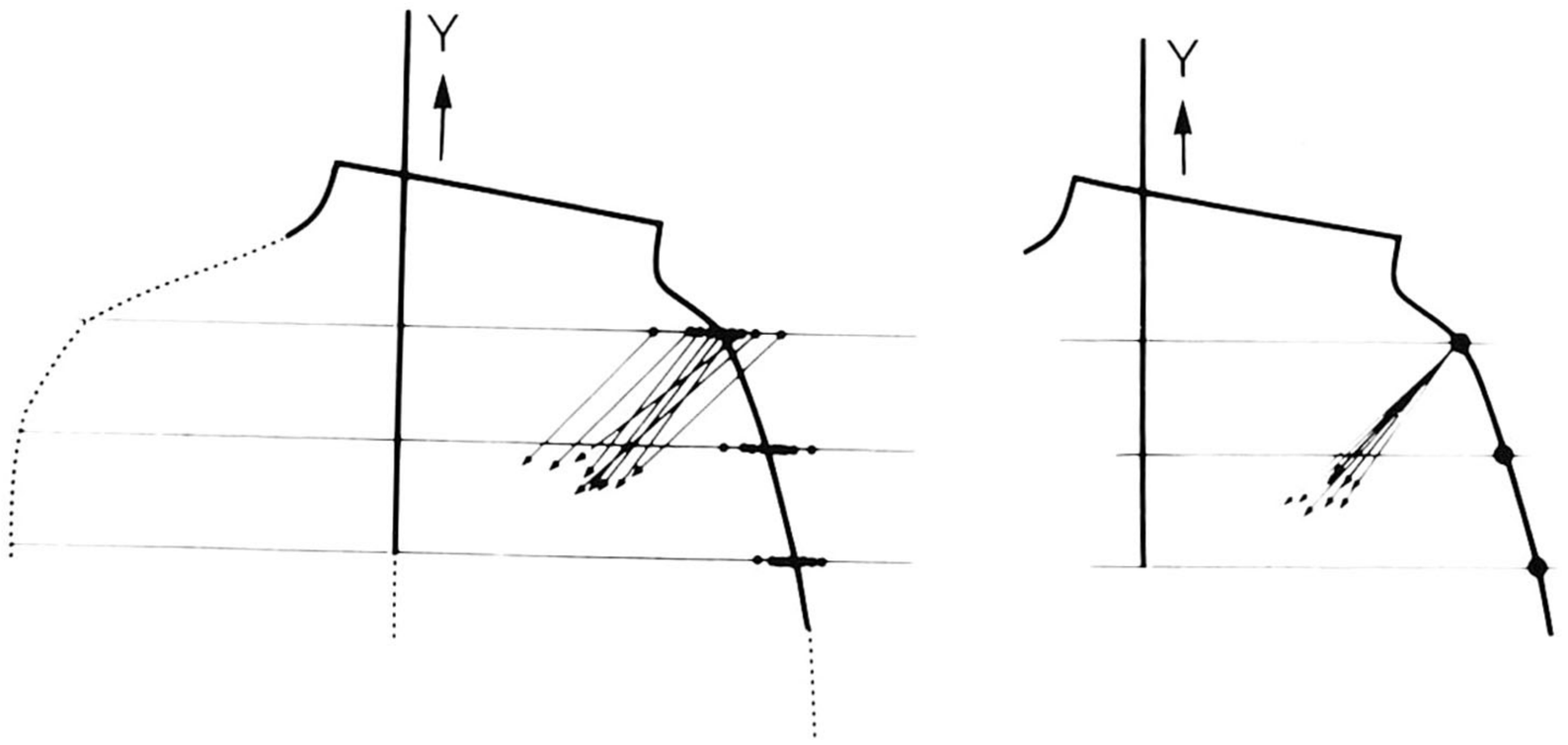

Figure 5. After normalization of the ventriculograms for long-axis length (**left**), corresponding starting points were shifted along the x axis so that they coincided, resulting in an x coordinate equal to the mean x value (**right**).

Statistics. By linear regression analysis, the extent and direction of the metal marker pathways, denoted as Δx_{metal}, Δy_{metal} and α_{metal}, were compared with the nearest corresponding endocardial (endo) landmark pathways, denoted as Δx_{endo}, Δy_{endo} and α_{endo}. Statistical analysis was performed with the Student's paired *t* test; values were considered significant at a probability (p) level of 0.05.

Results

Endocardial wall motion in pigs. Table 1 shows the mean and standard deviations, before and after metal marker insertion, of the hemodynamic variables left ventricular end-diastolic volume, ejection fraction, end-diastolic pressure, maximal rate of change in pressure (dP/dt) and heart rate. The hemodynamic changes were not statistically significant. After the experiment the myocardium was inspected visually at the position of marker insertion and no substantial damage, such as hemorrhage or cardiac rupture, was observed.

Figure 6 shows the normalized systolic pathways of the endocardial landmarks of each pig (1a to 8a) with the systolic pathways of the implanted metal markers of the same ventricles (1b to 8b). Comparison of the x and y components of corresponding pathways of endocardial landmarks (Δx_{endo} and Δy_{endo}) and of metal markers (Δx_{metal} and Δy_{metal}) results in a correlation coefficient of 0.74 and 0.86, respectively, with the linear regression equations as follows: $|\Delta x_{endo}| = 0.16$ cm $+ 1.2\ |\Delta x_{metal}|$ and $\Delta y_{endo} = -0.13$ cm $+ \Delta y_{metal}$ ($n = 41$). The relation between the directions of the endocardial landmark pathways and the metal marker pathways was similarly evaluated: $\alpha_{endo} = 0.86\alpha_{metal} - 2.9°$; $r = 0.86$; SEE $= 10.3°$ ($n = 33$). In this comparison the apical segments were excluded because the displacements of these segments have such short trajectories that accurate assessment of the acute angle and direction (α) is almost impossible.

In Figure 7 the normalized shape is shown for the end-diastolic left ventricular contours of the eight animals with the mean systolic pathways of the endocardial landmarks and their standard deviations as well as the mean pathways of the metal markers. Left ventricular long-axis length was 7.3 ± 0.4 cm.

Endocardial wall motion in humans. The coordinates of the 20 sites along the endocardial border can be used to define the normalized shape of the end-diastolic left ventricular contour. The mean and standard deviations of their x coordinates in the 23 normal human subjects are presented in Figure 8. The left ventricular long-axis length was 8.3 ± 1.3 cm. The mean systolic landmark pathways and their standard deviations are shown in Figure 9.

The points of intersection of the mean pathways extending from the 10 pairs of opposing end-diastolic sites with the x and y coordinates of the intersection points are depicted on the left side of Figure 10. For the second pair from the apical position, no point of intersection could be found within the ventricular cavity because of an almost parallel course of the opposing trajectories. The result shown in Figure 10 can be formulated so that for any point of an end-diastolic contour, the approximate mean direction of motion can be easily calculated. Consider L the length of the end-diastolic long axis as defined in Figure 4, (x_a, y_a) the co-

Table 1. Hemodynamic Data Before and After Metal Marker Implantation in Eight Pigs

	Control Period	After Marker Implantation	Statistical Significance
LVEDV (ml)	28.5 ± 5.2	29.4 ± 6.7	NS
EF (%)	61.4 ± 14.2	56.3 ± 12.0	NS
LVEDP (mm Hg)	10.5 ± 2.2	8.2 ± 3.7	NS
Peak dP/dt (mm Hg/s)	1,730 ± 278	1,436 ± 39	NS
HR (beats/min)	88 ± 5	87 ± 3	NS

EF = ejection fraction; HR = heart rate; LVEDP = left ventricular end-diastolic pressure; LVEDV = left ventricular end-diastolic volume; NS = not significant at a p value of 0.05 (*t* test).

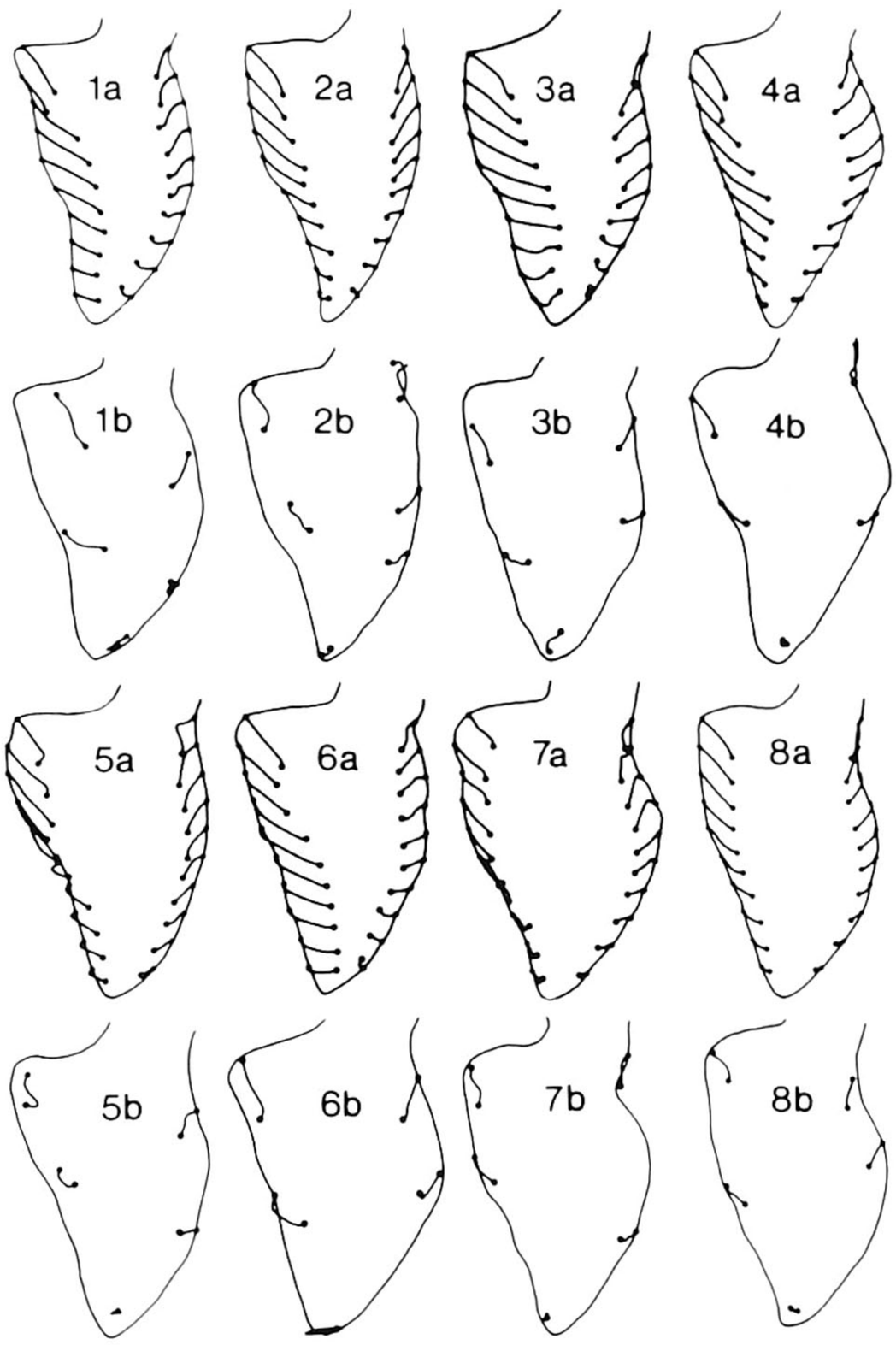

Figure 6. Normalized left ventricular systolic pathways (1a to 8a) of the endocardial landmarks in the eight study pigs are shown with the systolic pathways of the implanted metal markers (1b to 8b) in the same pig ventricles. Note the similarity of the pathways of the landmarks and the markers.

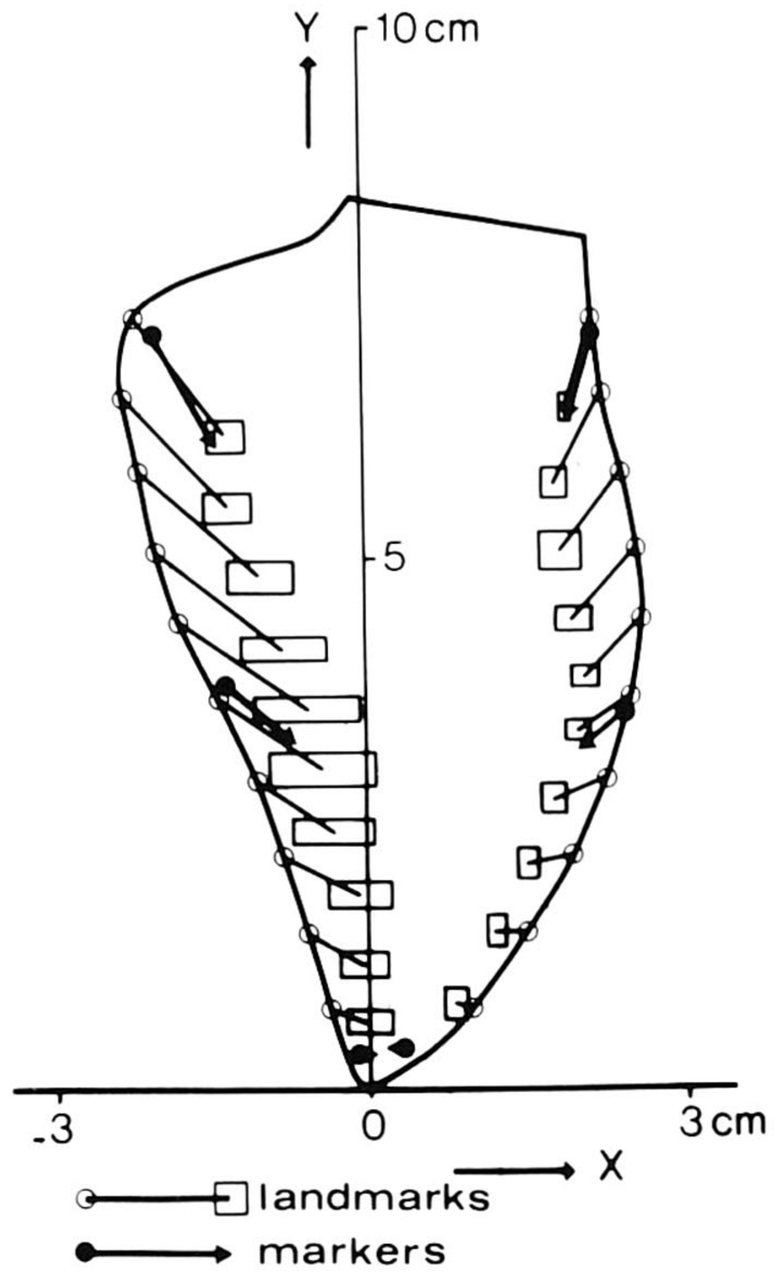

Figure 7. Mean normalized shape of left ventricular end-diastolic contours in the eight pigs. Left ventricular long-axis length is 7.3 ± 0.4 cm (mean ± SD). The mean systolic pathways of the endocardial landmarks with their respective standard deviations are indicated by **rectangles** and the mean metal marker pathways are indicated by **arrows.** Y and X = y and x axis, respectively.

ordinates of a point on the anterior wall and (x_i, y_i) the coordinates of a point on the opposite inferior wall so that $y_a = y_i = y$. In a first approximation, the coordinates (x_p, y_p) of the point toward which both opposite points will move are then defined by: $x_p = (x_a + x_i)/2$ and $y_p = L(0.57 - 0.53 \mid 1 - 1.1y/L \mid^{1.4})$.

Applying these formulas to the normalized contour of Figure 8 results in the positions shown on the right side of Figure 10. The difference between corresponding pathway directions on the left and right parts of Figure 10 is less then 4°, except for the 9.7° difference for the pathway starting from the mitral valve fornix.

Discussion

Landmarks. Quantitative analysis of left ventricular wall motion from angiocardiograms in humans has been hampered by the lack of an accurate and generally accepted

Figure 8. Normalized shape of the end-diastolic left ventricular contour of the 23 normal human subjects. Dimensions are expressed in centimeters. Left ventricular long-axis length is 8.3 ± 1.3 cm (mean ± SD).

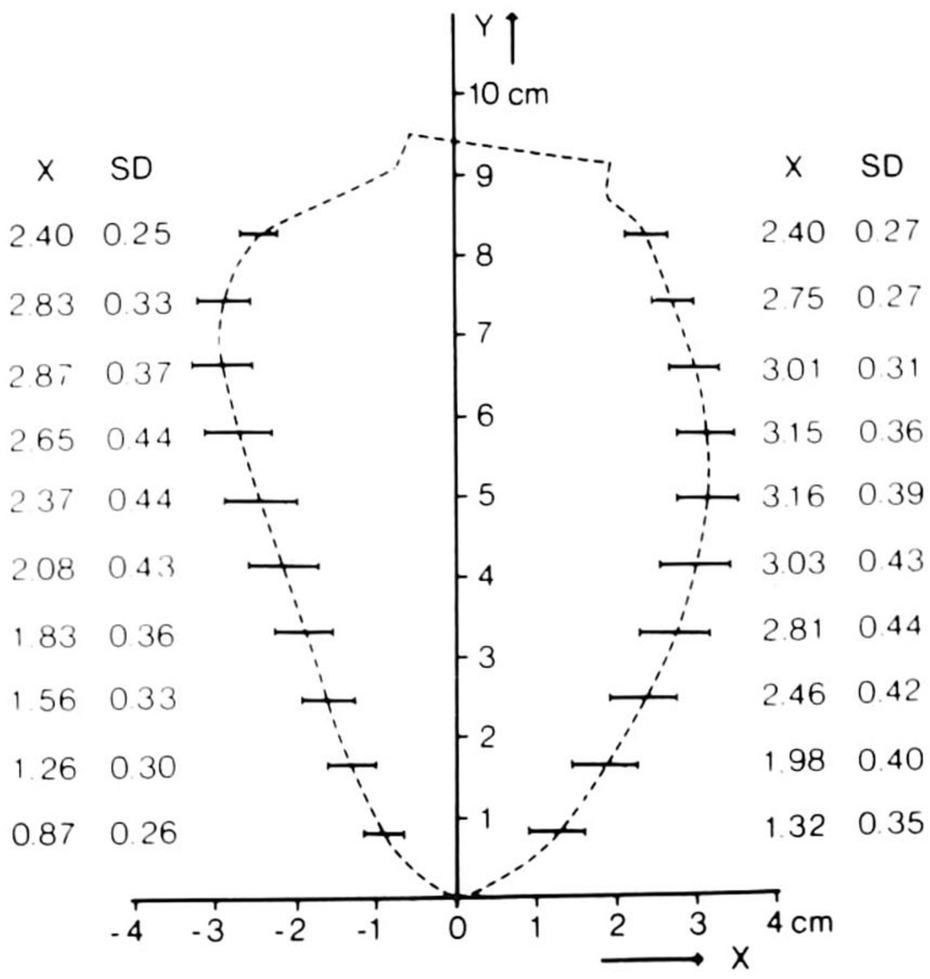

JACC Vol. 7, No. 2
February 1986:317–26

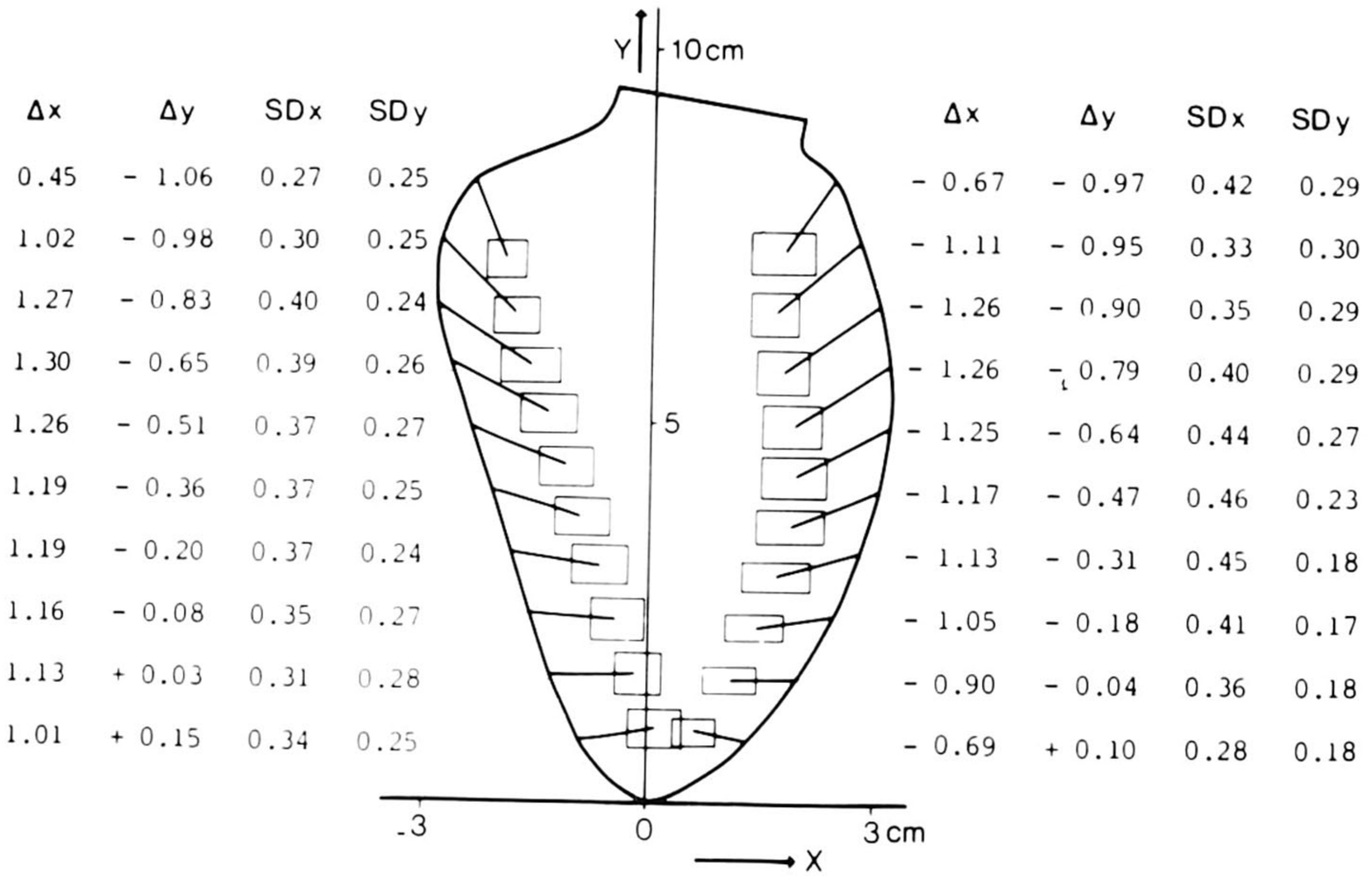

Figure 9. Mean systolic left ventricular endocardial landmark pathways in the 23 normal human individuals. The x and y components of each pathway are expressed as Δx and Δy. The **rectangles** represent the standard deviation (SD) of Δx and Δy.

procedure to define the direction of systolic motion of the endocardial border. Early experience with an automated endocardial outlining system (19) suggested that anatomic landmarks, appearing regularly in consecutive analyzed frames of the cineangiogram, could be followed over substantial portions of the cardiac cycle. Although not each individual landmark could be followed over the entire systolic period as rotation of the ventricle occurred along its long axis and while contrast medium is squeezed out of the intertrabecular spaces, it proved possible to interpolate between neighboring landmark pathways. Because neighboring landmarks are part of closely connected endocardial structures, they follow the same direction of motion as observed in the initially chosen projection. The aim of our study was to test this earlier hypothesis and to collect new data on endocardial wall motion that have not been available before. These data

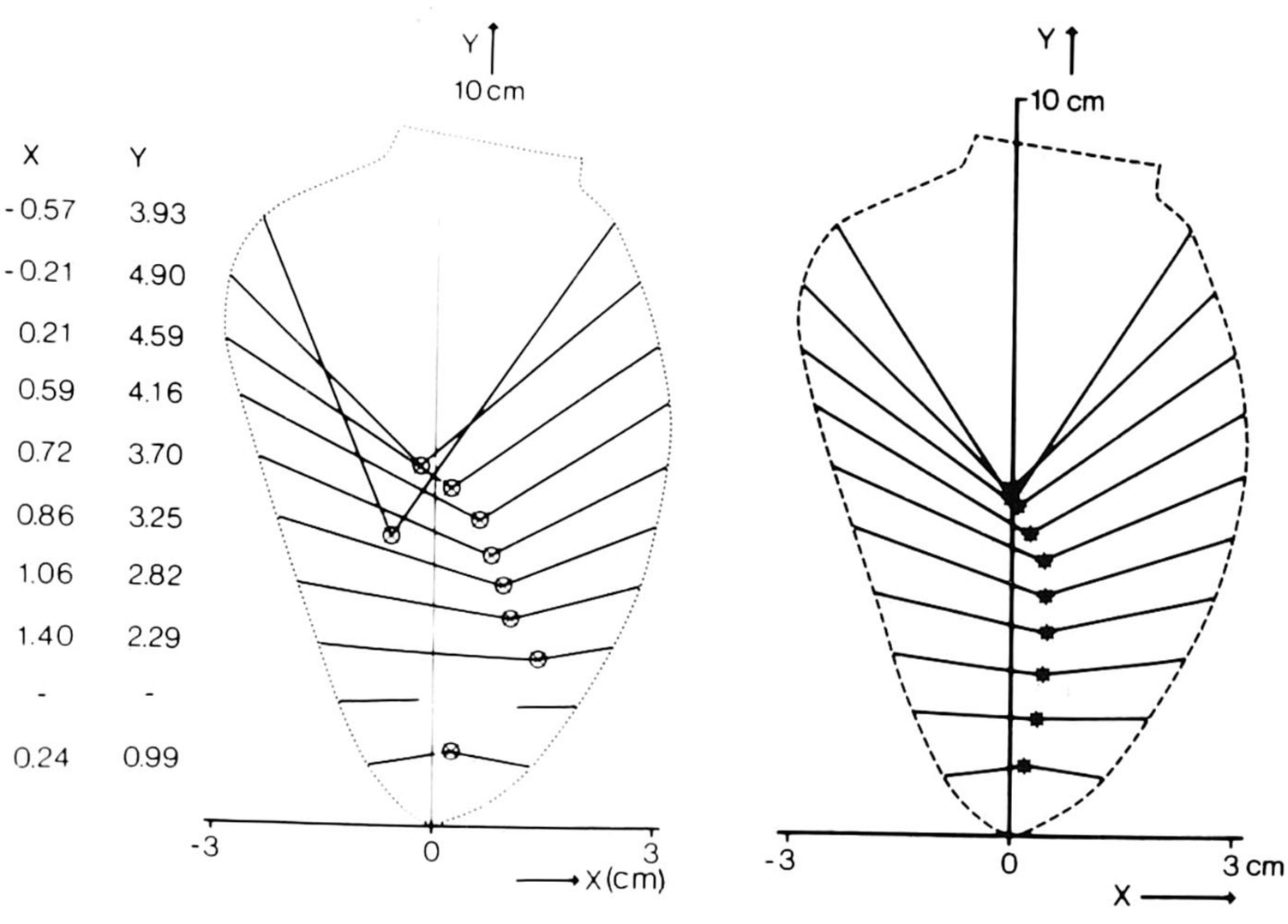

Figure 10. Points of intersection of the pathways extending from the 10 pairs of opposing starting points (**left**) and points of intersection of the pathways and direction of regional wall motion using the mathematical expression described in the text (**right**).

are needed for the further development of well founded methods for analyzing regional left ventricular wall motion.

Marker insertion. Analysis of the hemodynamic variables and the electrocardiogram before and after marker insertion revealed no sign of significant cardiac damage resulting from the procedure. In one pig a minor change in the T wave was observed. Visual inspection of the myocardium at autopsy revealed no significant damage at any site of marker insertion. In all cases the cylindrical marker was fixed exactly against the endocardial surface. The value of choosing the lateral projection of the left ventricle in the pig is evident because this view compares best with the right anterior oblique projection in humans (Fig. 2).

Angiographic properties. Linear regression analysis of the endocardial landmark and metal marker pathways in pigs showed an acceptable correlation coefficient for the y components ($r = 0.86$) but a much lower coefficient for the x components ($r = 0.74$). A significant difference was also found between the slopes of both regression equations: 1 and 1.2 for the y and x directions, respectively. This discrepancy can be explained by the apparent exaggerated endocardial inward motion, in a direction perpendicular to the endocardial wall, as observed on the contrast angiogram. This overestimation of systolic wall motion is caused by the squeezing of contrast medium out of the intertrabecular space in which the markers were usually inserted, and from the papillary muscle area, as has also been observed by others (1,12,20,21).The discrepancy in overall percent wall thickening among the reported results from the contrast medium methods (22–24), the bead and clip method (8) and the ultrasound crystal methods (25,26) also supports this view. For nearly all measured endocardial locations, the additional motion has a much larger x than y component and thus primarily influences the observed x components of most landmark pathways. The papillary muscle area of the pig left ventricle (Fig. 7) appears to be especially sensitive for this phenomenon. Comparison of the direction of motion of the endocardial landmarks and metal marker pathways shows a rather high correlation ($r = 0.86$) with a small standard error of the estimate of 10.3°. The slight underestimation of the acute angle (α) by the landmark pathways is also influenced by the exaggerated wall motion in the x direction.

Observer variability. A small, though definite intraobserver variability in the drawing of the landmark pathways exists, which further explains the uncertainty in the estimation of α and Δy. Earlier measurements (17) showed that the observer variability in the y direction of the landmarks is 1.4 mm (SD).

Ventricular shape. The variations among the different human ventricular shapes are distributed in a regular fashion over the entire ventricular wall (Fig. 8). They show a surprisingly narrow range. Variations in the valvular anatomy and in spatial orientation with respect to the X-ray system

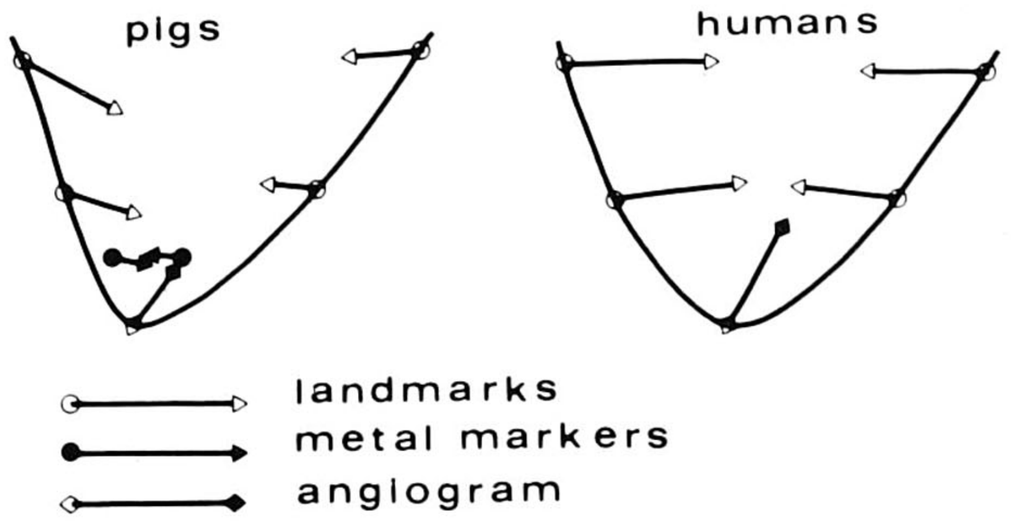

Figure 11. Mean systolic wall motion of human and pig left ventricles near the apex following metal markers, anatomic landmarks and the apical angiographic contrast border.

have almost no influence on the normalization procedure used in this study. Other ways of normalization usually lead to greater variations. If, for example, the junction of the mitral and aortic valves is chosen to define the y axis, it follows from our data that the deviations at the basal ventricular sites will be twice as large.

Normal wall motion. In humans and animals, the y components of the endocardial landmark trajectories show a gradually decreasing magnitude from base to apex. This is in agreement with the systolic descent of the base of the heart, as observed in animal experiments (7,27–29) and human studies (12,30). The apical landmark motion in the y direction is very small, although in many cases visual inspection of the contrast angiogram would suggest a con-

Figure 12. End-systolic frame of left ventricular cineangiocardiogram after marker insertion. The corresponding end-diastolic frame is shown in Figure 2. Squeezing of contrast medium from the apex may result in an apparent rotation and ascent of the apex as observed on the contrast angiogram, while the end-diastolic and end-systolic metal marker positions are almost identical (see Fig. 6b).

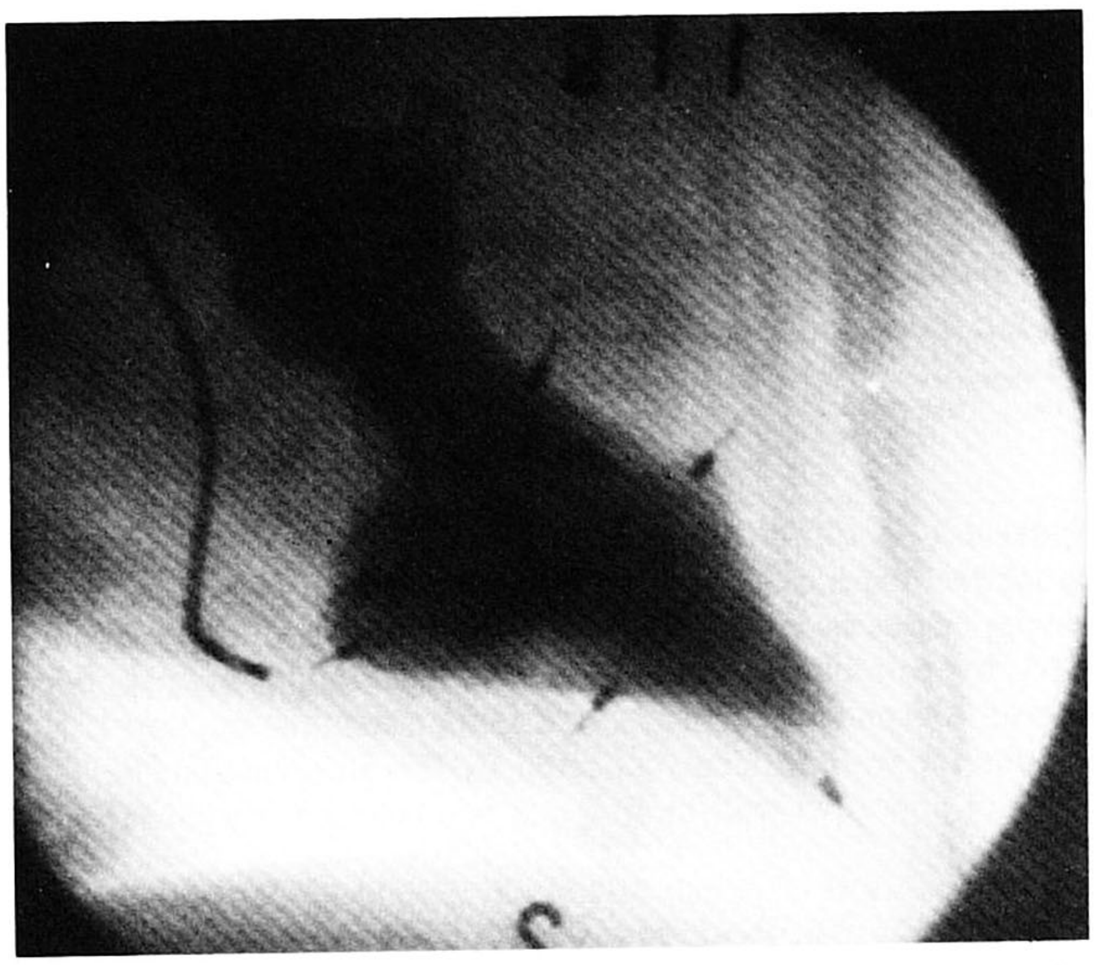

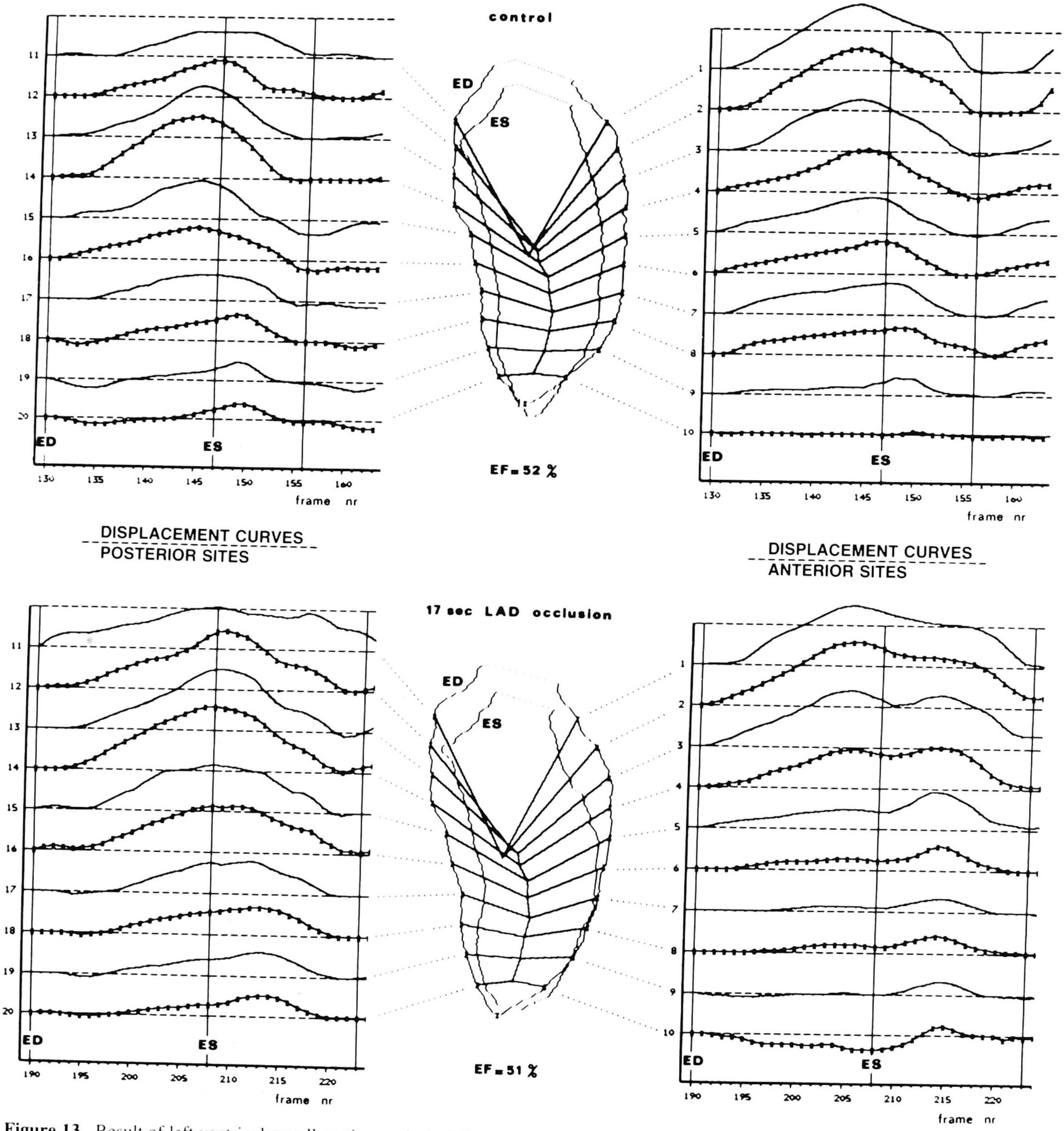

Figure 13. Result of left ventricular wall motion analysis following the landmark model before (**upper panels**) and during (**lower panels**) occlusion of the left anterior descending (LAD) coronary artery by balloon angioplasty in a patient with coronary artery disease. Despite the constancy of global ejection fraction (EF), the anterior wall is deeply affected by this intervention. Several stages of abnormal wall motion can be observed, varying from a typical U wave pattern at sites 3 to 4, a significant delay in the moment of maximal inward motion at sites 5 to 9 and even dyskinetic motion at apical site 10. In contrast, the inferoposterior wall (sites 11 to 20) shows an increase in the extent of inward wall displacement, but the pattern of motion at the various sites is practically unchanged. ED = end-diastole; ES = end-systole; nr = number.

siderable apical upward motion toward the base. In Figure 11 the apical motion of the pig and human left ventricles is shown in more detail. Note the apparent systolic upward motion of the apex resulting from the usual angiographic analysis method, which simply follows the moving contrast border. This situation is clearly demonstrated in Figure 12, which shows at end-systole the same ventricle shown at end-diastole in Figure 2. The apparent systolic upward motion is caused by complete extrusion of contrast medium from the apex and posterior papillary muscle area in late systole.

From the analysis of contrast angiograms in humans, many investigators erroneously concluded that the apex moves considerably toward the base during systole (2,4) and, consequently, they overestimated long-axis shortening (4,30). In addition, contrast angiograms in the right anterior oblique projection in particular suggest a substantial rotation of the apex along the left ventricular long axis. Earlier studies (7,12,27) with epicardial and endocardial markers had already shown that the apex is remarkably stationary during systole. Finally, a study in humans (6) with implanted midwall metal markers showed similar results.

Wall motion models. Several findings of our study have important consequences for the field of wall motion assessment from the angiogram. First, high accuracy cannot be expected in, for example, measurements of wall thickening because of the squeezing behavior of the wall. Second, as a result of this same behavior, the angiogram, because it primarily shows the displacement of the blood-dye mixture, may be even more sensitive than are implanted markers in demonstrating the effect of minor changes in regional wall function.

The choice of an external reference system to measure wall motion cannot be deduced simply from the results of this or other marker studies (31). However, it is clear that methods that are intended to correct for extracardiac motion are likely to introduce artifacts because they are dependent on the shape of the end-systolic contour. If, for example, the end-systolic apex is used to realign the ventricular long axis, a single inaccuracy in its determined position will greatly impair the accuracy of wall motion assessment at all ventricular sites. Furthermore, if regional wall motion is abnormal, the shape of the end-systolic contour will also deviate from normal. This also influences the correction procedure itself, with the result that displacement data from opposing ventricular walls will influence each other (32).

Landmark model. The mathematical description of the landmark pathway directions in humans can be used advantageously for the study of wall motion in general. The process of manually indicating the mitral valve fornix can be automated by means of the following algorithm. At first, the algorithm searches for an inscribed isosceles triangle with its vertex at the apex and having a maximal base length. Next, it determines an isosceles triangle with a base length equal to 78% of the determined maximum. This latter triangle (Fig. 4) is then used to define the required rectangular coordinate system with respect to which all subsequent calculations are performed. Because this implies that an external reference system is used, no means are available to discriminate between cardiac and noncardiac motion. Noncardiac motion can be avoided in clinical practice to a great extent by the control of respiration during filming. When used in an abnormally contracting heart, application of this generalized landmark model may introduce some error. This error will probably be minor because a subnormal regional contraction will result in a decrease of both the x and y components of the regional wall displacement vector. This will cause a decrease in extent, but not a major change in direction, of wall motion.

An example of the clinical application of the landmark model is shown in Figure 13. Wall motion is measured before and during occlusion of the left anterior descending coronary artery by balloon angioplasty. At 17 seconds of occlusion wall motion of the anterolateral and anteroapical areas deviates significantly from the control situation. With respect to the end-diastolic moment of maximal volume, the onset of displacement at sites 6 to 10 is delayed. The moment of maximal inward wall displacement, with respect to the end-systolic moment of minimal volume, is also delayed at sites 4 to 10. At sites 3 and 4 a typical U wave pattern can be observed. The apex shows dyskinetic motion. As a whole, the pattern of motion of the inferoposterior wall is only slightly affected by the intervention. The synchrony and the extent of motion show some improvement, which results in the preservation of global ejection fraction. The late inward motion at inferoapical sites 18 to 20 already exists during the control situation and is probably a sign of insufficient blood supply to this area. After the successful angioplasty procedure, apical inward motion increased and showed an improved synchronous motion with respect to the other sites at the inferoposterior wall.

Conclusions. The motion pattern of landmarks appearing at the endocardial border, as detected with an automated technique for the analysis of cineangiograms, appears to reflect the motion pattern of actual anatomic structures. From the analysis of results of normal landmark motion, a generalized model for endocardial wall motion has been derived that aids the further development of methods to quantify regional left ventricular function in clinical practice.

We gratefully acknowledge the assistance of Robert H. van Bremen and Marita A. Rutteman in performing the animal experiments and of Jan van Oosten of the University of Technology at Delft who constructed with great craftsmanship the marker insertion device.

References

1. Herman MV, Heinle RA, Klein MD, Gorlin R. Localized disorders in myocardial contraction. N Engl J Med 1967;227:222–32.

JACC Vol. 7, No. 2
February 1986:317–26

2. Leighton RF, Wilt SM, Lewis RP. Detection of hypokinesis by quantitative analysis of left ventricular cineangiograms. Circulation 1974;50:121–7.

3. Harris LD, Clayton PD, Marshall HW, Warner HR. A technique for the detection of asynergistic motion of the left ventricle. Comput Biomed Res 1974;7:380–94.

4. Rickards A, Seabra-Gomes R, Thurstone P. The assessment of regional abnormalities of the left ventricle by angiography. Eur J Cardiol 1977;5:167–82.

5. Chaitman BR, Bristow JD, Rahimtoola SH. Left ventricular wall motion assessed by using fixed external reference systems. Circulation 1973;48:1043–54.

6. Ingels NB, Mead CW, Daughters GT, Stinson EB, Alderman EL. A new method for assessment of left ventricular wall motion. In: Computers in Cardiology. Long Beach, CA: IEEE Computer Society, 1978:57–61.

7. Rushmer RF, Crystal DK, Wagner C. The functional anatomy of ventricular contraction. Circ Res 1953;1:162–70.

8. Mitchell JH, Wildenthal K, Mullins CB. Geometrical studies of the left ventricle utilizing biplane cine-fluorography. Fed Proc 1969;28:1334–43.

9. Carlsson E, Milne ENC. Permanent implantation of endocardial tantalum screws. A new technique for functional studies of the heart in the experimental animal. J Can Assoc Radiol 1967;19:304–9.

10. Ingels NB, Daughters GT, Stinson EB, Alderman EL. Measurement of midwall myocardial dynamics in intact man by radiography of surgically implanted markers. Circulation 1975;52:859–67.

11. Harrison DC, Goldblatt A, Braunwald E, Glick G, Mason DT. Studies on cardiac dimensions in intact, unanaesthetized man. I. Description of techniques and their validation. Circ Res 1963;13:448–67.

12. McDonald IG. The shape and movements of the human left ventricle during systole. Am J Cardiol 1970;26:221–30.

13. Brower RW, ten Katen HJ, Meester GT. Direct method for determining regional myocardial shortening after bypass surgery from radiopaque markers in man. Am J Cardiol 1978;41:1222–9.

14. Wildenthal K, Mitchell JH. Dimensional analysis of the left ventricle in unanaesthetised dogs. J Appl Physiol 1969;27:115–9.

15. Slager CJ, Reiber JHC, Schuurbiers JCH, Meester GT. Contouromat: a hardwired left ventricular angioprocessing system. I. Design and application. Comput Biomed Res 1978;11:491–502.

16. Chapman CB, Baker O, Reynolds J, Bonte FJ. Use of biplane cinefluorography for measurement of ventricular volume. Circulation 1958;18:1105–17.

17. Slager CJ, Hooghoudt TEH, Reiber JHC, Schuurbiers JCH, Booman F, Meester GT. Left ventricular contour segmentation from anatomical landmark trajectories and its application to wall motion analysis. In: Computers in Cardiology. Long Beach, CA: IEEE Computer Society, 1979:347–50.

18. Brower RW. Evaluation of patient recognition rules for the apex of the heart. Cathet Cardiovasc Diagn 1980;6:145–57.

19. Slager CJ, Reiber JHC, Schuurbiers JCH, Meester GT. Automated detection of left ventricular contour. Concept and application. In: Heintzen PH, Buersch JH, eds. Roentgen-Video-Techniques. Stuttgart: Georg Thieme, 1978:158–67.

20. Chapman CB, Baker O, Mitchell JH. Experience with a cinefluorographic method for measuring ventricular volume. Am J Cardiol 1966;18:25–30.

21. Hugenholtz PG, Kaplan E, Hill E. Determination of left ventricular wall thickness by angiocardiography. Am Heart J 1969;78:513–22.

22. Sandler H, Dodge HT. Left ventricular tension and stress in man. Circ Res 1963;13:91–104.

23. Eber LM, Greenberg HM, Cooke JM, Gorlin R. Dynamic changes in left ventricular free wall thickness in the human heart. Circulation 1969;39:455–64.

24. Dumesnil JG, Ritman EL, Frye RL, Gau GT, Rutherford BD, Davies GD. Quantitative determination of regional left ventricular wall dynamics by roentgen videometry. Circulation 1974;50:700–8.

25. Sasayama S, Franklin D, Ross J Jr, Kemper WS, McKown D. Dynamic changes in left ventricular wall thickness and their use in analyzing cardiac function in the conscious dog. Am J Cardiol 1976;38:870–9.

26. Osakada G, Sasayama S, Kawai C, et al. The analysis of left ventricular wall thickness and shear by an ultrasonic triangulation technique in the dog. Circ Res 1980;47:173–81.

27. Hamilton WF, Rompf JH. Movements of the base of the ventricle and the relative consistancy of the cardiac volume. Am J Physiol 1932;102:559–65.

28. Tsakiris AG, van Bernuth G, Rastelli GC, Bourgolis MJ, Titus JL, Wood EH. Size and motion of the mitral valve annulus in anesthetized intact dogs. J Appl Physiol 1971;30:611–8.

29. Hinds JE, Hawthorne EH, Mullins CB, Mitchell JH. Instantaneous changes in the left ventricular lengths occurring in dogs during the cardiac cycle. Fed Proc 1969;28:1351–7.

30. Brower RW, Meester GT. Computer based methods for quantifying regional left ventricular wall motion from cine ventriculograms. In: Computers in Cardiology. Long Beach, CA: IEEE Computer Society, 1976:55–62.

31. Clayton PD, Jeppson GM, Klausner SC. Should a fixed external reference system be used to analyze left ventricular wall motion? Circulation 1982;65:1518–21.

32. Ingels NB Jr, Daughters GT, Stinson EB, Alderman EL. Evaluation of methods for quantitating left ventricular segmental wall motion in man using myocardial markers as standard. Circulation 1980;61:966–72.